ASTRONOMY & ASTROPHYSICS
SUPPLEMENT SERIES

DECEMBER II **1999**, PAGE 309

Astron. Astrophys. Suppl. Ser. **140**, 309–326 (1999)

A survey of blue – Hα objects in the galaxy M 33

S. Fabrika and O. Sholukhova

Special Astrophysical Observatory of the Russian AS, Nizhnij Arkhyz 357147, Russia

Received June 18; accepted July 19, 1999

Abstract. For the purposes of a search for SS 433 type objects, LBV stars and hypergiants in M 33, we have carried out a photometry of blue stars in Hα images of this galaxy. From 2332 listed OB stars, we have isolated 549 objects, which have Hα excess over stars of the same V magnitude. Among them 81 emission stars (s) have been selected. About 60% of isolated objects found to be extended in Hα, among them 154 diffuse (d) and 180 bubble–type (b) nebulae. 117 objects are compact (c) and faint Hα sources. These groups are different in colour indices, Hα fluxes, surface brightness and sizes. The most probable size of the Hα nebulae is $FWHM = 10 - 14$ pc. There is evidence that their properties and location in the galaxy are defined by interstellar gas pressure and related to spiral arms. The d objects are H II regions with an embedded star. The b objects are probably envelopes around WR stars or SN remnants. Among s–type objects we isolated a group of 20 brightest stars, which in their average properties fit well to the parameters of blue hypergiants or LBV–type stars. The stars of intermediate brightness follow very well to blue Ia supergiants. The interstellar absorption derived from brightest Hα stars is $A_V = 0\overset{\mathrm{m}}{.}93 \pm 0\overset{\mathrm{m}}{.}05$. We classify the faintest stars as blue Ib supergiants, their average absorption is $A_V \approx 0\overset{\mathrm{m}}{.}6$. They are restricted in number by the limiting stellar magnitude in the original sample.

Key words: nearby galaxies: stellar content: individual (M 33): stars: early type — Hα excess

1. Introduction

This work has been done within frames of the program of a search for new unique stellar objects in nearby galaxies, which we initiated in (Fabrika & Sholukhova 1995). By unique or anomalously active objects we mean SS 433 — a massive binary system, where a supercritical gas accretion onto relativistic star occurs, LBV stars (Luminous Blue Variables — S Dor and P Cyg stars, Hubble–Sandage variables) that show superpowerful wind outflow, B[e] supergiants, bright WN stars. All these objects are young massive single or binary stars, brightest in the Galaxy. In their main spectral characteristics in optical range (blue continuum, bright Hα emission) these stars are similar to the object SS 433, free from interstellar absorption. Another common property of these stars is they all are massive stars in critical stages of evolution. Progress in understanding of physics and evolution of these stars could be made if we find as many as possible of stars of such types or similar stars. Most such stars in the Galaxy are obscured from the observer because of considerable absorption of light. That is why it is important to search for such objects in nearby galaxies.

The most suitable for our purpose are massive spiral, nearly face–on galaxies, the best example is M 33. It is important that this galaxy contains many young stars and it is well studied. Ivanov et al. (1993) (here and after IFM) have compiled a catalogue of OB stars up to $V = 19\overset{\mathrm{m}}{.}5$ in M 33. Assuming the number of early massive stars in M 33 to be about 2000, Fabrika & Sholukhova (1995) have estimated the expected number of SS 433 type objects between 1 and 20. In that paper we have discussed basic criteria of a search for such objects in M 33. These criteria are mainly associated with similarity to SS 433. The object has to be 1) OB star and 2) Hα star, as SS 433 itself is a very powerful Hα source. Additional criteria are 3) He II λ4686 emission, 4) a radio nebula associated with candidate star, 5) a possible X–ray source, 6) brightness variability in V–band up to 1^{m} on a time scale from days to years. Besides, Hα line may be strongly variable. SS 433 Hα line equivalent width changes from 100 to 1000 Å, while its FWHM is about 30 Å. Criteria 1, 2 and partly 6 are common to SS 433 and LBV type stars, that is why it is worthwhile to make a concurrent search for such objects. The principal point is the existence of an early–type star with a strong (and possibly broad) emission line Hα. That is why it seemed natural to extend the work and carry out a systematic search for all stars of the

above–mentioned types on the basis of selection of objects by the criterion OB star + Hα emission.

Based on all above enumerated criteria, Fabrika & Sholukhova (1995) have made a cross–correlation analysis and selected 171 stars to be candidates for unique objects (the list I). When making up this list we made a cross–correlation of coordinates of OB stars from IFM and star–like Hα sources from Courtes et al. (1987). In the list I were also added 19 early stars with $V \leq 18^m$, which are visible on the Hα images (Courtes et al. 1987) as stars brighter than the majority of OB stars of the same magnitude in V. The selection criterion was $\triangle m \gtrsim 1^m$ (Fabrika & Sholukhova 1995). This selection was based on visual estimates, therefore the list of OB–Hα stars in the list I (Table 6 in the quoted paper) is rather incomplete. In this paper we examine OB stars in Hα images on the base of photometry of all objects from IFM. This catalogue comprises 2112 stars up to $V = 19\overset{\text{m}}{.}5$ which have been selected by the criteria $U-V < 0, U-B < 0$. When we started this work we used the 1st version of the catalogue (kindly made available by G. Ivanov prior to publication). We have supplemented it with new additional objects from published version. So we have studied Hα images a total of 2332 blue stellar objects. It is not improbable that these objects include star–like nebula too, as well as compact groups of stars.

2. Photometry of Hα images, selection of candidates

We have used Hα photographs (contact copies) obtained by Courtes et al. (1987) on the 6 m telescope with a focal reducer f/1. The Hα band had a width $FWHM = 35$ Å, the contribution of the nitrogen lines [N II] $\lambda\,6548, 6584$ is estimated as less than 10%. The scale of the images is $34\overset{''}{.}5$/mm, the angular resolution is about $1''$. All the images were digitized with a square diaphragm of 20 μm and a step of 20 μm (one pixel = $0\overset{''}{.}68$).

We made a search for all blue stars on the Hα images, using their accurate coordinates. Even with the finding chart taken from B band images (IFM) being available, it is far from being always possible to identify Hα objects, because of the dominant contribution of nebula and the strong and nonuniform Hα background. We used the coordinate grid (Fabrika & Sholukhova 1995) whose accuracy is $0\overset{''}{.}3$. From stars and objects, which are positively identified for certain, the coordinate grid was transferred to the Hα images. The accuracy achieved was about $1''$, which is better than that of the original catalogue (IFM) equal to $1\overset{''}{.}5$. All the catalogue star positions were plotted on the Hα images with a three–fold error boxes ($\pm 4\overset{''}{.}5$). The objects that fell against a very strong background were not considered. We could make the Hα photometry for 1619 out of 2332 cataloque stars. From our estimates, the limiting stellar magnitude of a reliably measured OB star, which has no intrinsic Hα emission and is located in the outlying parts of the galaxy, is $V = 18.5 - 19.0$.

The photometry was performed with the program package developed by V.V. Vlasyuk (personal communication). The objects selected were measured with square diaphragms whose size was increased from 3 to 30 pixels with a step of 2 pixels ($1\overset{''}{.}36$). The integral density in the diaphragm and background density along the diaphragm's perimeter were measured. For the following study we used density D, which is equal to the difference between total density inside chosen diaphragm and background density (average background per pixel multiplied by the diaphragm area). The object size ($FWHM$) was found in the following way. The level of half–intensity with subtracted background was found, and then the area at this level was put equal to an area of a circle with a diameter $FWHM$. Besides that, for the sake of inspection, the size was also determined through a fitting of an object profile with the Gaussian in two orthogonal sections. Hereafter we will call the density as a flux F, which is measured in our relative units. As a rule, with a diaphragm size increasing both the integral flux and the object size grow, then these values get a plateau. The ordinate of the plateau is just a measured quantity. The dependence of relative flux error $\sigma(F)/F$ on the flux shows that for faint objects the error does not exceed 10%, for the main body of the objects it does not exceed 5%. The size error is less than 30% at $FWHM \approx 2''$, less than 20% at $3''$ and below 5% at size greater than $5''$. We also tested a possible influence of an object position in the image (the edge effect) on the size measured accuracy. This could readily be done since the images were obtained (Courtes et al. 1987) with an overlap of $2' - 3'$. Analysis has shown that the change in the size of a star, as dependent on its position in the image, is well under the size measurement accuracy. To diminish the personal error, any procedure described in this paper has been performed by a single person. For more detail description of the photometry see Fabrika et al. (1997).

Quite an essential point of our work is that we measured not the intensities but the densities. The measured flux (density) may be related to the intensity in a complicated fashion through two characteristic curves, original and copy. This fact does not have any effect on the selection of the stars having Hα line flux excess over the stars of the same V magnitude and in the same image, which is the principal result of the work. The relationship between the flux and intensity may be both linear, $F \propto I$ and logarithmic, $F \propto \lg I$, depending on which part of the effective characteristic curve we work. The former is the most likely case since we measure very faint objects, therefore it is quite possible that we are working in the region of underexposures.

In Fig. 1 a relationship between flux F and magnitude V is presented for 148 stars of the eastern part of M 33 (image N 6 from Courtes et al. 1987). In this plot one sees distinctly the basic sequence of the stars without emission (filled circles) having no Hα excess. The sequence reflects the fact that the stars that are brighter in V band are

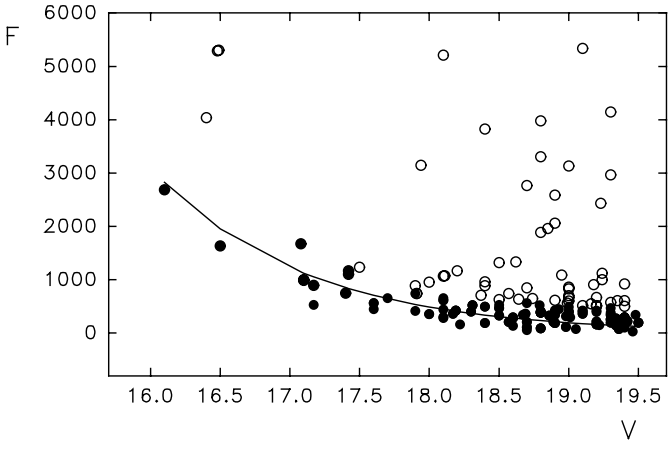

Fig. 1. Hα line flux F versus V magnitude for 148 measured stars of the image No. 6 of the eastern part of M 33. The stars selected by the criterion of flux excess are shown by open circles, the stars that comprise the basic sequence of nonemission stars — by filled circles

brighter in the Hα band. In our case the flux in the Hα band will depend on magnitude V as $F = a\,10^{-(0.4\,m_V)}$, if the stars are on the lower ("nonlinear") part of the effective characteristic curve, and as $F = b - c\,0.4\,m_V$ or $F \propto \lg I$, if the stars are on the logarithmic ("linear") part of the curve. Approximations have shown that the first relation is valid. The exponential function satisfies the location of stars on the basic nonemission sequence much better than the linear. This means that we are working in the region of underexposures on the effective characteristic curve, where $F \propto I$. However, as we have already noted, the result of the selection of stars that have excess in Hα (open circles) does not depend on this dilemma.

The selection of candidates was performed in the following manner. In the intervals $\triangle m_V = 0.5$, the mean Hα flux value and its standard deviation were found. The stars, whose flux was greater than the mean flux over $2\,\sigma$, were rejected. The remaining objects have been fitted with the curve $F = a\,10^{-(0.4\,m_V)}$, and the stars with a deviation greater than $2\,\sigma$ were rejected, then the fitting was repeated. The described procedure converged after 2–3 iterations. The "cleaned" basic sequence of the nonemission stars $F_{\rm b}(m_V)$ and its rms deviation $\sigma_{\rm b}(F)$ were thus obtained. Then stars from the original data whose flux departed from it upwards by a value greater than $2\,\sigma_{\rm b}(F)$ were isolated. Application of this procedure distorts a little the basic sequence statistics. Nevertheless we used it because the procedure converges very well, and the final selection criterion is rather arbitrary. This criterion, $S \geq 2$, where $S = (F - F_{\rm b})/\sigma_{\rm b}$, is a "soft" enough, and it has been chosen in order to not miss possible interesting stars with a weak Hα emission. The selected stars are the objects sought with a flux excess in the Hα over OB stars without emission by a value higher than $2\,\sigma_{\rm b}$ of the basic sequence scatter. The same methods were applied for all the images from Courtes et al. (1987). All in all 549 objects were selected as a result of the Hα photometry of 1619 blue stars from IFM.

3. The flux–size and surface brightness–size relationships

The early stars with Hα emission we have isolated may have either intrinsic emission (the objects of our search), or be stars in H II regions. In the nebulae the central ionizing star visibility in V band depends on the contribution of the nebula lines to this band. After spectroscopy of the objects it will be possible to answer the question, however, examination of Fig. 2 can considerably clear up the situation. On the plot Hα flux — size for all measured objects of the image No. 6 (small circles) the objects are readily seen to be divided into two (or probably three) branches. It is natural to connect this division with different morphological types of the objects: the lower sequence represents "stars", the upper (or two upper sequences) — "nebulae" or "stars plus nebulae". On the image there appeared to be about 60% extended objects, 20% of stellar objects and also about 20% of the objects located in the lower–left corner of the diagram of Fig. 2 at the point of a junction of all branches.

It is known that a compact H II region can imitate a hot star in the $U - B$, $B - V$ colours and may also be a star–like source (in M 33 $1'' = 3.5$ pc). Nebulae (or nebulae with a visible star) may well be included in the catalogue of hot stars IFM. For star–like objects the flux must be $F \propto 10^{\alpha d}$, where d is the size of a star on a plate (Zickgraf & Humphreys 1991). In the case of a supernova remnant or a bubble–type nebula, $F \propto d^2$, and in the case of a filled or a diffuse nebulae, $F \propto d^3$. An intermediate power sequence is also possible depending on the morphology of a nebulae and a star contribution to the Hα band.

The results of testing this interpretation are contained in Fig. 2. We plot there from the same image a number of objects, whose morphology is obvious: apparent but not bright stars (triangles), large bubble–type nebulae (squares), "core plus halo"–type nebulae and diffuse nebulae (circles). The small circles indicate the objects from Fig. 1. It is seen from Fig. 2 that the stars indeed fall in the lower stellar sequence, bubbles — in the uppermost sequence (to be more precize, in its continuation). The third, intermediate sequence is continued by diffuse and "core plus halo" nebulae. All three sequences join naturally in the region of objects' sizes $1'' - 2\farcs5$.

The apparent separation of the objects in Fig. 2 provides grounds to break up all the studied objects on the basis of their morphological features in Hα into sequences: stars, bubble nebulae and intermediate diffuse (or complex) nebulae. The objects having low fluxes and small sizes are common to all three sequences. We label these 4 groups by s, d, b and c, respectively. It should be emphasized that the division can be done only on the average.

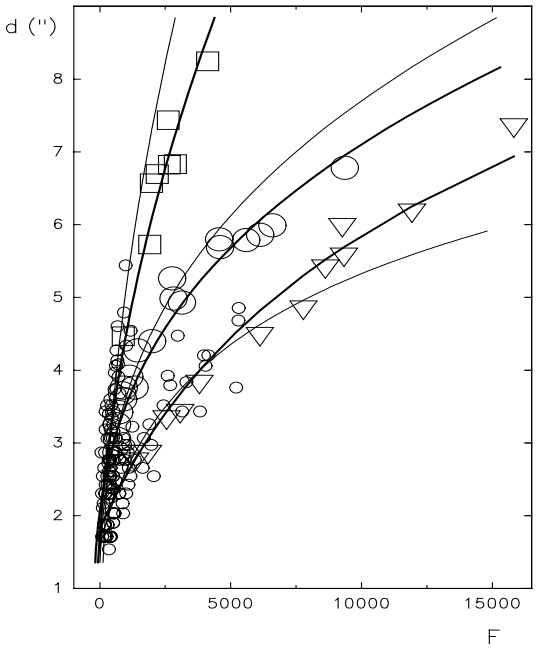

Fig. 2. An object size $FWHM$ as a function of Hα flux for the same stars as in Fig. 1 (small circles). There are also shown brighter stars (triangles), obvious nebulae — bubbles (squares) and diffuses (large circles) from the same image. Bold lines show approximations of the sequences with bright stars and nebulae included, thin lines are those for the studied objects only

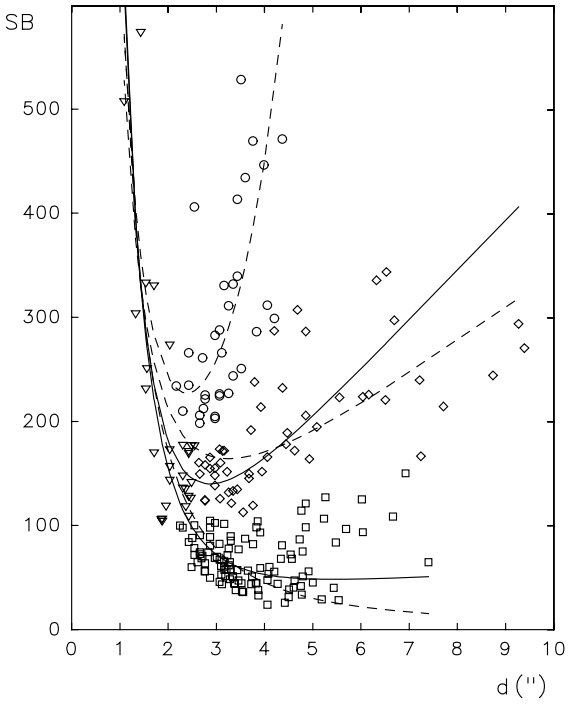

Fig. 3. Relationship between Hα surface brightness and a size for objects from image N 2. Stars — circles, diffuse nebulae — diamonds, bubbles — squares, common point–like objects — triangles. Approximations of the isolated sequences are shown by dashed lines and those with allowance for the photographic effect by solid lines

Some of the objects fill space between the sequences, which is caused not only by photometric errors, but by the real complex morphology of the nebulae.

We made approximations of each of the isolated sequences in Fig. 2 with the inclusion of the objects of known types (bold lines) and only for the objects under study (thin lines). The objects of type c were added, when approximating, to all three sequences. For both versions of the stellar sequence $F = b + F_0 \cdot 10^{\mathrm{ad}}$ turned out optimum. By equalling the flux to zero, we find an estimate of the seeing size d_0 in a given image. In particular, in Fig. 2 $d_0 = 1\farcs8$ and $1\farcs6$ for all stars and for the catalogue stars, respectively.

The bubble sequence must satisfy $F \propto d^2$. A formal search for the best curve fitting this data with the power function $F \propto d^n$ yields $n = 1.95 - 2.05$, i.e. the square power does fit this type of objects. Approximations of two samples — with inclusion of the known bubbles and without them by $F = a + F_0 \cdot d^2$ yields a good fit, a formal seeing estimate is $1\farcs7$.

Approximations of the intermediate type (diffuse) nebulae are also presented in Fig. 2. One may propose that the appearance of the diffuse sequence may be due to inaccuracies in determining the parameters of objects of complex structure. However, the fact that the bright diffuse nebulae fit well the intermediate sequence is a forcible argument in favour of reality of the intermediate objects as a separate diffuse sequence. Approximation of this sequence by $F \propto d^n$ yields $n = 3.2 \pm 0.3$, i.e. the cubic power describes well the diffuse branch (the formal seeing estimate there $d_0 = 2\farcs0$).

It should be noted that the approximation results prove in themselves that we are working on a nonlinear part of the effective characteristic curve. We have found that this is valid at least in $F < 7000$, and practically all the objects under our study are faint enough to be underexposed. The images of central region of the galaxy, however, are characterized by a stronger background and their position on the effective characteristic curve could be shifted a little to the linear region, where $F \propto \lg I$. However the fact that the both fits (bold and thin lines in Fig. 2) are very similar gives us a proof that we may use the approximation $F \propto I$ for all objects under study. When examining the rest of the images, we applied quite similar techniques. The conclusions drawn from a single Hα image were confirmed for the remaining 8. The seeing estimate for all the photographs is $1\farcs8 \pm 0\farcs1$, which is in agreement with the real seeing value during the observations (Courtes et al. 1987).

A relationship between a size d and surface brightness $SB = F/d^2$ has been also studied for the selected candidates. Such a plot for one of the central images is presented in Fig. 3. As was to be expected, the objects broke up

into three sequences according to these described above. In this representation, some of the objects of type c are easier to identify and refer to one of the sequences s, d or b. We made the approximations in Fig. 3 (dotted lines) using the objects broken up into sequences s, d, b separately and also those c–type objects, which are close to the each sequence:

$$SB = \begin{cases} (a + c10^{\alpha d})/d^2 \\ (a + cd^3)/d^2 \\ (a + cd^2)/d^2, \end{cases}$$

where the coefficients a, c and α were determined for each sequence and in each image separately.

The curves in Fig. 3 fit well the sequences (on average), especially the star sequence — the upper curve in the figure. Nevertheless it is quite possible to improve the fits for the extended objects. For this purpose the photographic effect of a star size growing with star brightness has to be taken into account. This is most essential for nebulae of small sizes. From the analysis of Fig. 3 it can be concluded that with nebulae sizes of $2''-4''$, the curves (two lower dotted lines) overestimate the value of SB, i.e. the data themselves are located, on average, below the curves. To allow for this effect, it has to be added to the formula of the nebulae flux ($F(d) = A + F_0\, d^n$) a term, which describes the behaviour of a point–like source, $F(d) = (A + B\, d^{2n} + C \cdot 10^{\beta d})^{1/2}$. Taking $F_0\, d^n$ out of brackets and expanding the rest into a series with $d = d_0$, one can find that the allowance for the photographic effect can be made by adding to the flux expression, a linear term $F(d) = A + F_0\, d^n + kd$. The solid lines in Fig. 3 show the b and d–type object approximations with the linear term allowed for. Agreement between the curves and the data for the nebulae is seen to considerably improved. With the aid of the diagram SB–d we managed to isolate a part of the objects from the group c and refer them to one of the three morphological sequences.

4. The list

Thus, all Hα excess objects were divided into sequences on the basis of their morphological features: stellar (s), diffuse (d), bubble–type (b). Faint and compact objects that remained unclassified were labeled by c. Besides this, there were objects for which it turned out to be impossible to determine the size because of their closeness to bright H II regions. As a rule, in Hα images, these objects are seen as a hump near a large nebula, i.e. they are located on a steep background gradient. In the methods we used, their size would often be underestimated or formally equal to zero. We denote such objects as zs. As a result there were isolated 81 stars, 154 diffuse nebulae, 180 bubbles, 117 objects of type c and 17 zs objects. The division between s and d, d and b objects have to be considered as an average, but not precise, because there are some objects located between the sequences and the objects may obviously have not a simple Hα morphology.

All isolated objects are listed in Table 1, where the columns present: 1) successive numbers n, 2) number from the original catalogue n(IFM). The last 35 objects are from the first unpublished version of the catalogue. Other columns are 3) stellar magnitudes V, 4) $S = (F - F_\mathrm{b})/\sigma_\mathrm{b}$ — flux excess over the flux of the basic (nonemission) star sequence, which is measured in standard deviations of stars composing this sequence, 5) object sizes in arcseconds (for objects of types b and d only), 6) morphological type. Finding charts could be found in IFM.

From the examination of Table 1 it follows that the objects having a maximal excess in Hα belong mostly to the diffuse nebulae sequence, while the objects with a minimal excess belong to the sequence of bubbles (see also Table 2). On the basis of the photometry data we may estimate Hα line flux in units of stellar continuum flux. One may find a quantity $W'_{\mathrm{H}\alpha} = \triangle\lambda \cdot ((F - F_\mathrm{b})/F_\mathrm{b})$, where $\triangle\lambda = 35$ Å is a width of Hα band used (Courtes et al. 1987). It is important to note that F is a total Hα band flux which is radiated both in a whole nebula and in a star's atmosphere, but the continuous emission F_b is stellar. In a case of pure intrinsic stellar Hα emission it is the line equivalent width. In a case of nebula emission, $W'_{\mathrm{H}\alpha}$ is a direct function of the star UV luminosity beyond Lyman edge over that in V band, i.e. it is a function of the ionizing star's temperature. In general case $W'_{\mathrm{H}\alpha}$ depends on H II region size that surrounds the star, which in turn is determined by the star's temperature and luminosity, electron density and other parameters of the medium. The object sizes and the Hα fluxes measured, may be of independent interest for study the isolated nebulae and their central stars parameters.

Calzetti et al. (1995) published results of a systematic search for SS 433–type candidates in the galaxy M 33. To isolate candidates they used CCD images of M 33 in a narrow Hα band and in an adjacent continuum at about 6100 Å. They have estimated a limiting stellar magnitude as $V \approx 20$. The M 33 field coverage by their images is approximately twice as small as the region we have studied. Calzetti et al. (1995) have isolated a total of 279 compact H II regions and 153 point–like emission sources (actually analysis of their images reveals that their samples contain 27 object repetitions). Their fields contain 311 objects from 549 objects we have selected. Comparing our Table 1 with the data of Calzetti et al. (1995), we found 42 common objects, 17 of them among H II regions and 25 from the point–like emission objects. The greater part of these H II regions belong to our sequence of diffuse nebulae. A half of these point-like Hα sources are also among our diffuse nebulae, while the rest of the objects are of types s and c. The list of Calzetti et al. (1995) comprises 64% H II regions and 36% point–like objects. Our sample

Table 1. Selected emission objects

n	n(IFM)	m_V	S	$d(''$)	Type	n	n(IFM)	m_V	S	$d(''$)	Type
1	8	18.80	3.7	3.0	b	41	208	17.00	10.6		s
2	11	18.50	6.6		c	42	210	18.47	6.0	4.0	d
3	18	18.40	5.7	2.8	d	43	211	17.97	4.6	3.2	b
4	22	18.60	2.9	3.2	b	44	215	18.60	13.4	3.1	d
5	42	18.70	52		s	45	216	18.81	42	6.0	b
6	60	19.10	34	4.6	d	46	222	17.70	5.9	3.0	d
7	61	19.20	68	6.9	b	47	227	18.90	2.5	3.9	b
8	65	16.67	7.5		s	48	228	18.35	5.8	4.2	b
9	68	19.30	10.0	5.4	b	49	240	17.20	32	4.4	d
10	71	19.00	5.2	3.2	b	50	246	18.70	2.1	5.5	b
11	72	18.65	23	3.7	d	51	248	18.39	2.6		c
12	87	18.00	6.4	3.1	d	52	263	17.81	13.5	3.7	d
13	90	18.31	3.2		c	53	268	17.30	42	6.7	d
14	99	18.58	3.2	2.7	b	54	272	18.10	4.8	3.3	b
15	101	18.24	6.5		c	55	276	16.80	7.4	3.9	d
16	104	18.70	3.2		c	56	282	19.10	8.7		c
17	109	18.80	14.3		s	57	284	19.19	7.1	3.0	b
18	116	18.20	16.2		s	58	285	19.42	6.0		c
19	119	18.60	12.9	3.1	d	59	298	18.60	24		s
20	120	18.70	5.8		c	60	301	16.40	4.0	4.1	d
21	125	19.22	12.5		s	61	329	18.80	1.9		c
22	131	17.80	61	5.6	d	62	337	19.10	2.0		c
23	136	19.50	11.6	3.3	d	63	341	19.40	6.2		c
24	137	17.79	390		zs	64	343	17.83	6.5	5.7	b
25	139	17.70	10.8		s	65	344	18.90	12.4	3.8	d
26	140	18.70	3.6	3.8	b	66	350	19.02	3.0	2.7	b
27	141	18.80	8.4	2.6	d	67	352	19.30	83	9.0	d
28	143	18.40	5.8		c	68	361	19.00	18.6		s
29	147	18.40	1.9	3.5	b	69	366	18.40	2.9	4.0	b
30	156	19.48	2.8	3.1	b	70	368	17.80	15.9		s
31	162	18.91	5.4	4.5	b	71	369	19.38	17.7	3.7	d
32	168	18.40	13.2	4.8	b	72	372	19.10	7.8		s
33	169	17.71	5.6	2.9	d	73	374	17.12	11.0		s
34	172	19.00	2.1	2.8	b	74	382	18.33	11.2	4.4	b
35	174	18.79	6.7	4.8	b	75	383	19.19	4.6		c
36	188	17.70	2.9		c	76	386	17.30	8.3		s
37	192	17.61	10.0		s	77	392	19.30	7.3		c
38	200	19.48	3.8	4.9	b	78	401	17.70	2.6	3.0	d
39	202	19.27	82	6.2	d	79	403	19.47	40	5.3	d
40	205	19.49	2.5	4.1	b	80	404	16.90	14.1		s

contains 63% d and b nebulae, 15% s and 22% c objects, i.e. 37% are star–like emission objects. The relative proportions of extended and star–like objects in these two lists are in agreement. The incomplete overlapping of the lists is likely to be due to the fact that Calzetti et al. (1995) have examined central regions of M 33, where the great Hα background inhibits the separation of emission objects in the photographic data we used. For this reason these two lists may be considered as complementing each other.

5. Types of selected objects

Let us investigate in more detail the different types of Hα objects. In Table 2 we present their mean photometric parameters. The columns give morphological types of objects, their numbers, stellar magnitude V, colour indices $U-B$, $B-V$ (IFM) and $V-$Hα, surface brightness (Hα flux per square arcsecond), Hα excess parameter S, size of objects and $W'_{\rm H\alpha}$. Stellar magnitude in Hα is not calibrated and it has been derived from the relative flux in this band, $m(\mathrm{H}\alpha) = -2.5 \lg F(\mathrm{H}\alpha)+24.5$. It should be borne in mind that the flux F(Hα) depends directly for extended objects on a nebula size, but this is not the case for stars as point sources.

As distinct from the continuous spectrum of stars, where there is a direct relationship between colour indices and temperature of a star, the colours of a nebula depend on a number of factors including the ionizing star temperature, electron density, dilution factor (size of a nebula), optical depth. Besides, colours may vary in a complex manner depending on the reddening. The

Table 1. continued

n	n(IFM)	m_V	S	$d(''$)	Type	n	n(IFM)	m_V	S	$d(''$)	Type
81	406	19.36	5.6	3.9	b	121	548	16.80	15.3		s
82	408	19.10	9.3		c	122	550	19.20	84		s
83	409	18.68	26	5.2	b	123	555	18.80	2.2	3.3	b
84	411	18.00	10.3	3.4	d	124	559	17.72	5.3		s
85	412	18.60	29	5.1	d	125	561	17.69	5.0		s
86	417	19.21	3.3	3.1	b	126	571	17.58	19.9		s
87	420	19.42	4.5		c	127	574	19.16	6.1		c
88	422	19.01	25		s	128	578	19.10	9.2	4.4	d
89	424	19.00	68	7.1	d	129	584	18.97	3.1	3.1	b
90	425	19.34	8.9	4.2	d	130	589	18.22	20.0	5.8	d
91	426	17.20	5.9	3.2	d	131	592	18.60	24.8	5.1	d
92	431	17.99	2.3		c	132	607	19.42	4.7		c
93	432	19.21	3.2		c	133	609	18.66	5.6	5.5	b
94	435	17.60	6.8	3.5	d	134	611	17.00	8.9	5.3	d
95	442	18.50	2.1	3.3	b	135	614	17.20	9.3		s
96	444	17.28	9.8		s	136	619	17.40	9.3	4.1	d
97	449	18.78	4.9	4.8	b	137	629	19.40	36	7.3	d
98	452	19.17	4.1	4.3	b	138	630	18.70	6.7	3.6	d
99	454	18.90	2.8	5.3	b	139	633	19.30	117	10.5	d
100	455	18.39	31	7.4	b	140	637	18.75	4.4	3.6	b
101	465	18.68	2.1	3.4	b	141	639	18.40	13.7	4.9	d
102	466	19.33	22.9	5.5	b	142	644	17.90	4.2	4.1	b
103	467	18.40	2.8		c	143	646	19.11	7.3	3.5	d
104	471	19.10	170		zs	144	648	18.10	2.7	3.5	b
105	482	18.96	28	5.7	b	145	651	19.17	3.9	3.2	b
106	488	19.20	61	6.5	d	146	653	18.90	11.7		s
107	490	18.22	2.2		c	147	656	19.42	7.5		c
108	492	18.95	5.4	5.2	b	148	663	19.46	2.8	3.1	b
109	493	19.40	18.6	7.7	b	149	664	18.50	20.3	5.9	d
110	500	18.10	2.7	3.2	b	150	666	19.34	30		s
111	505	18.15	3.1		c	151	667	19.00	4.1	4.5	b
112	511	18.70	13.2	4.5	d	152	669	17.70	4.2		c
113	515	16.50	2.1	4.0	d	153	675	19.40	11.4		s
114	526	18.70	4.9	3.6	b	154	676	18.50	2.6		c
115	527	18.62	2.6		c	155	677	19.50	4.4		c
116	532	18.85	14.0	7.7	b	156	678	18.70	42	9.3	b
117	533	18.60	250		zs	157	689	19.20	2.8		c
118	536	19.43	2.4		c	158	697	18.17	2.7	3.8	b
119	537	18.60	7.7	4.3	b	159	699	18.00	17.4	4.9	b
120	544	17.90	8.2	4.2	d	160	701	16.99	34	4.9	d

intensity of hydrogen Balmer lines does not depend strongly on the nebula temperature. Together with hydrogen lines, the forbidden lines [O III] λ 4959, 5007 are the most intensive ones in the spectra of nebulae and a good indicator of electron temperature of gas (Allen 1973). They are approximately equal contributors to B and V bands. Other strong lines do not fall within V band. In B band are the intensive lines of a hot gas: Hβ, [Ar IV] λ 4712, [Ne IV] λ 4725, He II λ 4686, [O III] λ 4363 and [Ne III] λ 3967, 3969. The last two lines make about the same contribution to U band. There is the line [O II] λ 3727 in U band. With growing electron temperature and excitation of the nebula gas, the flux in B band will dominate. Accordingly the value of $U-B$ will increase while $B-V$ will decrease.

It is seen from Table 2 that in $U-B$ and $B-V$ the diffuse objects differ greatly from the bubbles. This is also displayed in Fig. 4. From the colours the diffuse nebulae are cool, their behaviour in the figure resembles the behaviour of the stars but the diffuses have a lower value of $U-B$. This may be due to the emission Balmer jump and the strong hydrogen lines in their spectra. The latter is suggested also by the large value of S in the diffuse nebula (Table 2).

In contrast to the diffuse objects, colour indices of bubbles indicate that the gas excitation degree in them is high. Besides, the objects of type b are, on average, considerably fainter in V than the diffuse nebulae. The location of these objects on the diagram in Fig. 4 suggests that they are clearly different in excitation and that the central star is a minor contributor to the spectrum. If the heating of such nebulae is radiative, the stars having a relatively small size must be sufficiently hot. It is unlikely, however, that these b nebulae sizes are defined at all by

Table 1. continued

n	n(IFM)	m_V	S	$d(''$)	Type	n	n(IFM)	m_V	S	$d(''$)	Type
161	705	19.00	19.8	4.5	d	201	821	19.00	7.8	4.1	d
162	710	19.00	10.7	4.9	d	202	823	18.80	10.7	4.9	b
163	712	17.68	63	7.2	d	203	825	18.10	6.4	4.3	b
164	714	18.84	3.7	3.4	d	204	830	19.10	5.1		zs
165	718	18.40	8.5	3.9	d	205	836	19.00	6.9	4.4	b
166	719	16.90	9.8	4.8	d	206	837	18.90	8.2		zs
167	727	16.80	16.2		s	207	839	16.70	3.6		zs
168	730	18.70	13.5	4.9	d	208	842	18.80	13.1		zs
169	734	18.40	6.0		c	209	844	19.20	3.6		c
170	735	19.00	61	7.9	d	210	853	19.30	9.7	4.5	d
171	736	16.40	15.5	5.9	d	211	856	17.90	8.8	3.3	d
172	740	18.80	6.9	4.2	b	212	861	18.90	53	8.5	d
173	743	15.87	3.2		s	213	863	18.60	4.0	2.9	d
174	747	19.36	60	8.7	d	214	867	18.84	3.9		c
175	749	19.30	7.6		zs	215	868	18.30	12.0	4.4	d
176	750	16.77	6.7		s	216	870	19.00	36.3	8.9	b
177	751	19.40	7.3		c	217	874	18.66	8.9	4.3	d
178	755	17.84	3.0	3.5	b	218	875	18.90	8.7	5.0	b
179	757	17.20	9.7	4.8	d	219	878	18.10	5.7		s
180	760	18.70	2.0		c	220	879	18.60	2.4	3.5	b
181	761	18.20	2.2		c	221	884	18.22	16.8	4.7	d
182	771	18.10	2.8		c	222	895	18.48	3.1		c
183	772	19.01	38	6.4	d	223	905	18.60	6.6	4.4	b
184	774	18.90	8.5	4.6	b	224	910	19.30	14.9	5.3	d
185	775	19.10	2.4		c	225	913	19.20	2.7	3.4	b
186	779	18.20	6.0		c	226	920	17.50	11.9	5.0	d
187	780	18.60	6.3	5.0	b	227	923	18.40	9.7	4.0	d
188	781	18.91	4.0	3.5	b	228	926	18.30	240	9.3	d
189	783	19.40	2.1		c	229	933	19.20	6.2		zs
190	784	18.80	3.3	3.2	b	230	935	19.20	15.6		s
191	786	18.30	6.3		c	231	936	19.10	2.9		c
192	789	19.20	27.5	6.2	d	232	938	17.50	7.0	4.0	d
193	790	18.85	2.1		c	233	948	18.38	6.0		s
194	791	18.80	5.2		zs	234	953	19.40	3.7		c
195	795	18.50	3.3		c	235	956	17.90	10.6		s
196	799	19.00	57.8	7.6	d	236	965	19.31	2.4		c
197	803	19.13	2.3		c	237	976	18.30	6.1	4.2	b
198	805	17.10	33.2		s	238	987	19.29	7.7	4.4	b
199	815	19.00	6.0	4.1	b	239	990	19.00	48		s
200	818	19.20	5.0	3.3	d	240	994	19.43	3.2	3.8	b

the central star's temperature and luminosity (see below Fig. 9). In the gas excitation collisional processes have to be dominating. From their specific Hα morphology (bubbles), colour indices, low luminosities, as well as their sizes and surface brightness behaviour (see below) we can refer them to envelopes around WR stars and SN remnants.

No less than 80% of WR stars in the Galaxy are embedded in H II regions (Lozinskaya 1992), and no less than 40% having ring nebulae. If the bubble-type nebulae surround WR and Of stars, then in heating and excitation mechanisms they may be similar to planetary nebulae. In this case we propose that a star itself could be not seen in the visible region of the spectrum and the observed emission is produced by the nebulae. In the case of extremely hot central stars of planetary nebulae, the star is fainter than the nebulae by $\triangle B = 6^m$, and at the star temperature of about 3 10^4 K the star is fainter by $\triangle B = 0\overset{\mathrm{m}}{.}4$ (Allen 1973). It can also be concluded that on U, B and V plates these objects must look like diffuse ones. That is why the largest of these objects are likely to be missing in the catalogue (IFM). It may be for the same reason the b nebulae have smaller sizes than d ones.

In the group c (faint and compact objects) all types of objects are probably present, however, compact diffuse nebulae are apt to be the most numerous among them. It is very remarkable that the zs–type objects that have been classified as a separate group only by Hα image morphology have the bluest index $U-B$, the reddest index $B-V$ and they are the most powerful Hα sources (see Table 2). Maybe these are compact H II regions with a very high gas density, with hydrogen emission lines of a nebula being a powerful contributor to the spectrum.

Figure 5 shows the relationship between the standard colours indices and $V-$Hα. In this figure and those

Table 1. continued

n	n(IFM)	m_V	S	$d(''$)	Type	n	n(IFM)	m_V	S	$d(''$)	Type
241	995	19.49	5.3		c	281	1130	19.20	3.3	4.5	b
242	999	16.46	2.1		s	282	1131	18.30	19.8	5.8	d
243	1001	18.73	11.5		s	283	1142	18.10	15.6		s
244	1002	16.20	2.9	4.2	d	284	1145	18.02	5.1	4.1	b
245	1003	18.20	2.5		c	285	1147	18.89	7.7	5.5	b
246	1004	16.40	6.2	5.3	d	286	1153	18.90	4.6		c
247	1005	19.10	9.4		s	287	1156	18.00	19.8	6.2	d
248	1006	17.60	5.6	3.5	d	288	1157	18.70	29	6.3	d
249	1010	19.38	2.4	3.1	b	289	1161	18.80	5.4	3.5	d
250	1011	19.20	2.7	2.9	b	290	1163	17.50	6.6	3.1	d
251	1013	19.20	19.6	5.7	d	291	1166	19.29	3.1		c
252	1018	18.40	3.1		c	292	1176	19.09	5.9		c
253	1020	17.90	25		s	293	1177	18.30	12.4	3.9	d
254	1022	18.80	2.8		c	294	1179	18.70	32	6.4	d
255	1024	17.70	28		s	295	1194	19.00	3.7	3.1	b
256	1026	16.60	17.5	5.5	d	296	1203	18.50	7.0	4.1	b
257	1030	19.30	5.1		c	297	1211	18.60	91	9.4	d
258	1031	19.30	9.0		zs	298	1212	19.00	5.5		c
259	1035	19.38	29	5.5	d	299	1215	19.50	14.9	4.7	d
260	1038	18.50	4.1		c	300	1216	18.30	3.3		c
261	1042	19.47	18.7		s	301	1219	18.50	10.1	3.9	d
262	1051	19.50	5.0		c	302	1222	19.23	33	4.4	d
263	1053	18.44	2.8	3.3	b	303	1228	18.70	6.5	4.5	b
264	1055	18.50	2.4	4.3	b	304	1242	18.39	3.7		c
265	1061	16.40	7.9		s	305	1248	19.40	9.8		c
266	1066	19.40	3.8		c	306	1249	18.00	7.7	5.8	b
267	1070	18.10	2.2	3.4	b	307	1254	17.71	5.8	3.7	d
268	1080	18.00	3.1		c	308	1263	19.50	13.8	4.8	d
269	1089	19.10	31		s	309	1265	17.81	7.1	3.8	d
270	1090	18.50	6.8		zs	310	1269	18.60	2.4	3.7	b
271	1097	18.20	17.6		s	311	1270	18.70	14.5	4.4	d
272	1101	18.50	3.7		c	312	1277	19.40	5.2	3.3	b
273	1102	19.20	20.8	5.7	d	313	1278	19.10	109	10.4	d
274	1104	19.20	4.1		c	314	1281	19.10	7.1	4.2	b
275	1105	19.50	9.7	4.7	b	315	1288	19.20	12.7		s
276	1106	18.80	7.8		s	316	1299	18.90	4.9	6.1	b
277	1112	19.10	2.3	3.2	b	317	1300	19.10	7.0	3.6	d
278	1122	18.20	3.0		c	318	1304	19.20	4.4	3.3	b
279	1123	19.40	4.9	3.5	b	319	1309	18.90	2.1		c
280	1129	18.50	3.0		zs	320	1314	16.90	10.6	4.0	d

followings the stars are designated by dots and their approximations by solid lines, the diffuse nebulae by rhombs and dotted lines, the b nebulae by squares (if shown) and longdashed lines. Here and further in the analysis of such relationships we use the linear function $y = C_x + C_1$ and present only the value of C and its rms deviation. The stars in Fig. 5 behave as one may expect: with increasing blue excess the intensity of Hα grows. For the stars $C(U-B, V-\mathrm{H}\alpha) = -0.085 \pm 0.035$ and $C(B-V, V-\mathrm{H}\alpha) = -0.083 \pm 0.029$. These relationships for the nebulae of b and d types differ considerably from those of stars, which confirms that these are the objects of different nature. Only in the diffuse nebulae a significant dependence is observed, $C(U-B, V-\mathrm{H}\alpha) = -0.109 \pm 0.019$, which is likely to be due to the growing size of the H II region with increasing temperature of the exciting star.

In Fig. 6 a distribution of the selected objects according to the galactocentric distance $R_{\rm gc}$ is displayed, that is the number of objects within the distances intervals. The corresponding distributions of the object numbers per unit area would be similar, but it would have quite a strong peak at small $R_{\rm gc}$, which would make it difficult to analyze. The object coordinates were deprojected from the picture plane onto the galactic plane. It was adopted according to Vaucouleurs (1959) that the inclination angle of the galactic rotational axis to the line of sight $i = 55°$ and the position angle of the major axis is PA = 23°. It is important to note here that in the central regions of the galaxy the real density must be higher. The selection effect is due to identification problems against the strong

Table 1. continued

n	n(IFM)	m_V	S	$d(''$)	Type	n	n(IFM)	m_V	S	$d(''$)	Type
321	1319	19.20	3.2		c	361	1473	17.70	4.8	5.4	b
322	1326	19.20	4.4		c	362	1474	17.70	9.1	4.9	b
323	1327	17.50	6.2	4.0	b	363	1475	19.00	3.2		c
324	1328	18.80	2.6	3.3	b	364	1480	18.80	4.5		c
325	1331	18.40	4.7	4.8	b	365	1487	18.50	9.2	4.3	d
326	1334	18.71	3.5	3.3	d	366	1504	18.93	3.4	3.3	b
327	1339	18.80	3.6		c	367	1507	19.40	4.3		c
328	1356	17.64	6.7	3.8	d	368	1508	19.10	64		zs
329	1358	18.50	8.2	4.1	d	369	1512	19.40	4.5	4.7	b
330	1363	19.30	35	4.5	d	370	1523	17.80	7.4		s
331	1368	19.07	28.3	5.4	d	371	1524	17.60	5.8	3.8	d
332	1381	19.00	36	6.8	d	372	1527	18.10	2.7		c
333	1383	18.90	3.3	5.7	b	373	1528	18.70	3.1		c
334	1386	18.60	6.7	3.9	d	374	1533	19.10	14.5		s
335	1389	18.90	3.7	3.9	b	375	1536	19.30	5.8		s
336	1393	19.20	3.8	3.2	b	376	1539	19.30	150	9.2	d
337	1396	19.20	2.5		c	377	1541	19.00	2.8	2.9	b
338	1400	19.00	39	10.7	b	378	1543	18.80	5.8	5.2	b
339	1402	18.70	84	9.1	d	379	1547	18.80	47	4.2	d
340	1404	17.50	7.1	3.2	d	380	1548	19.00	5.2	4.5	b
341	1405	19.40	100	9.9	d	381	1551	18.50	9.3	4.2	d
342	1406	18.61	119	10.2	d	382	1553	18.10	8.5	2.9	d
343	1408	19.41	2.4	4.2	b	383	1556	18.99	5.7	4.6	b
344	1413	17.20	11.9		s	384	1560	19.40	4.1	3.3	b
345	1414	18.10	3.9	3.4	d	385	1561	19.00	3.3	2.5	b
346	1422	18.70	3.5		c	386	1567	19.30	2.9	3.6	b
347	1426	18.90	7.9	4.6	b	387	1568	19.27	9.2		c
348	1427	17.90	3.5		c	388	1569	19.42	3.4	2.7	b
349	1431	18.09	7.5	4.5	d	389	1571	18.00	2.8	3.0	d
350	1434	18.65	4.3		c	390	1573	17.40	8.7	4.3	d
351	1436	19.40	2.5	2.9	b	391	1575	16.60	27	5.5	d
352	1440	19.00	2.1		c	392	1576	19.00	2.7	3.6	b
353	1448	18.60	2.0	3.4	b	393	1579	18.00	64		s
354	1451	18.40	2.2		c	394	1588	16.48	45	4.7	d
355	1453	18.40	5.6	4.4	b	395	1589	19.50	4.6	3.6	b
356	1460	18.99	5.3	3.5	d	396	1607	18.10	3.4		c
357	1463	18.40	3.5		zs	397	1613	19.30	5.0		s
358	1465	18.80	2.2		c	398	1617	18.31	2.6		c
359	1466	18.50	4.1	3.1	d	399	1625	18.79	4.0	2.9	b
360	1467	17.95	5.5		s	400	1630	19.10	2.6	2.5	b

Hα background of the central parts (the first $1-2$ bins in Fig. 6). This selection is about the same for all types of objects, however it affects mainly the diffuses and bubbles, whose average surface brightness is not high. It follows from the figure that the three types of objects belong to different populations. The distribution of emission stars along the radius is relatively uniform. The observed minima in the distribution (if even they are real) are insignificant in our data and could be random. The density of stars falls by a factor of 2 at $R_{1/2} \approx 4.2$ kpc ($1'' = 3.5$ pc). The diffuse nebulae distribution is quite different, they are located, on average, closer to the centre, $R_{1/2} \approx 2.4$ kpc, and they show a single significant maximum at 1.8 kpc.

The objects of type c are not presented in Fig. 6, they resemble most of all the diffuse nebulae. The nebulae of type *b* exhibit the most broad distribution with $R_{1/2} \approx 4.7$ kpc. It has two maxima at 2.9 and 4.5 kpc. The maxima are formally insignificant, however, the bubbles distribution itself is considerably more irregular than that of the diffuse ones (with about the same number of objects). It is not improbable that these maxima display that predominantly spiral arms fall within the defined intervals of galactocentric distances, or possibly they are due to ring structures in the galaxy. Another remarkable detail in Fig. 6 is that maxima in the distribution of stars and diffuse nebulae fall within the regions $1.4-2.1$ and $3.5-4.2$ kpc ($400''-600''$and $1000''-1200''$, respectively) and coincide with the minima in the distribution of bubbles. This matter is discussed below.

Thus, a number of characteristics: colour indices, surface brightness, distribution in the galaxy suggest that s, b and d objects are physically different. For instance, in $V-$Hα the b and d nebulae differ by 8σ (Table 2). Location of these objects over the galaxy is not uniform.

Table 1. continued

n	n(IFM)	m_V	S	$d(''$)	Type	n	n(IFM)	m_V	S	$d(''$)	Type
401	1637	19.30	14		s	441	1779	18.40	23.1		s
402	1644	17.10	3.0	3.8	d	442	1780	18.82	205		zs
403	1648	18.50	3.1	3.9	b	443	1781	19.30	4.3		c
404	1650	19.30	6.5	4.1	b	444	1783	19.20	30	6.5	d
405	1660	18.20	9.6	3.6	d	445	1790	19.01	60	7.6	d
406	1661	19.37	4.4	3.7	b	446	1793	19.00	2.8		c
407	1665	19.38	21	6.2	d	447	1794	18.86	2.2	4.5	b
408	1667	19.11	7.8	4.7	b	448	1796	18.40	8.3	3.0	d
409	1670	19.50	2.8	2.9	b	449	1800	19.00	88	6.5	d
410	1671	18.90	5.4		c	450	1805	18.11	8.6	3.0	d
411	1677	19.01	3.4	3.3	b	451	1808	19.19	5.6	3.7	b
412	1685	19.20	4.6		c	452	1810	18.70	32	6.4	d
413	1686	19.16	5.0	3.3	b	453	1811	19.10	3.2	2.7	b
414	1700	19.20	4.6	2.5	b	454	1813	19.40	51	7.5	d
415	1701	18.40	8.2	5.4	b	455	1818	18.90	23		s
416	1704	18.51	2.3	3.9	b	456	1820	18.64	5.0	2.9	b
417	1707	19.20	3.5	3.7	b	457	1821	18.80	2.8	3.2	b
418	1708	18.90	30	3.9	d	458	1825	17.08	13.7		s
419	1714	19.00	37	4.9	d	459	1829	19.20	6.6	4.6	b
420	1720	18.90	4.6	3.8	b	460	1838	19.30	5.8		c
421	1728	19.10	16.8		s	461	1840	19.40	120	7.7	d
422	1731	18.10	16.1		s	462	1852	19.30	5.6	2.9	b
423	1733	16.70	10.6	5.0	d	463	1855	18.85	22		s
424	1734	19.18	4.7	3.8	b	464	1866	18.90	3.4		c
425	1735	16.40	430		zs	465	1867	18.50	13.1	3.8	d
426	1736	19.50	2.5		c	466	1870	19.35	6.0	3.1	b
427	1737	18.20	4.1	2.9	b	467	1875	19.10	4.5	3.2	b
428	1741	18.40	2.6	3.1	b	468	1878	19.10	2.2		c
429	1747	18.70	4.2		c	469	1895	18.34	7.7		c
430	1749	19.30	8.3	4.6	b	470	1897	19.20	2.7	3.5	b
431	1750	19.10	61		s	471	1900	18.10	3.4	3.6	b
432	1751	16.40	27		s	472	1904	19.00	6.6	4.1	b
433	1761	19.10	33		s	473	1909	19.48	3.0	3.4	b
434	1764	19.30	2.7	2.6	b	474	1913	18.66	46	5.1	d
435	1765	19.40	6.6		c	475	1914	18.96	11.5	3.3	d
436	1766	18.20	10.2	4.5	b	476	1915	19.40	130	6.7	d
437	1770	19.26	2.7		c	477	1922	18.80	2.3	2.4	b
438	1775	18.26	2.0		c	478	1923	18.80	2.3	2.8	b
439	1776	16.49	45	4.9	d	479	1925	19.00	8.2	2.7	d
440	1777	19.38	3.4	4.4	b	480	1930	19.19	4.2	3.0	b

6. The nebulae

About 60% of emission objects in the survey possess the characteristics of nebulae. We may compare the new nebulae with already known ones in M 33. The fullest list was compiled by Courtes et al. (1987) that contained 748 Hα nebulae classified according to morphological properties. We used the same images taken with the 6 m telescope. Courtes et al. (1987) picked out the nebulae by visual inspection of the images, whereas our nebulae were found in computer photometry. In the former case the sample must contain the largest nebulae with dimensions of more than at least a few arcseconds. In our case we have nebulae of no more than a few arcseconds in size so far as the basis of the list is provided by objects (IFM) having nearly star–like images in B and V bands.

Figure 7a presents distributions of sizes for 334 nebulae of types b and d from Table 1 and 748 nebulae from the sample of Courtes et al. (1987). We restrict ourselves to sizes $\leq 40''$, which is sufficient for our study. Both distributions are normalized to the total number of objects in each sample. Maxima of these distributions are markedly different. The nebulae found with the visual inspection of the images has a wide maximum in region of $5''-12''$. It is evident that its location is determined by the selection of incomplete inclusion of nebulae smaller than $\approx 10''$ in size. Our nebulae maximum falls at sizes $3''-4''$, which corresponds to $10-14$ pc. Estimates of the most likely size of H II regions in M 33 are known from $4''.5$ (Sabbadin et al. 1980) to $13''$(Boulestex et al. 1974). The most likely size derived depends on a number of factors, mainly on image scale (see review and discussion in Sharov 1988). It is improbable that distribution of real nebulae sizes

Table 1. continued

n	n(IFM)	m_V	S	$d(''$)	Type	n	n(IFM)	m_V	S	$d(''$)	Type
481	1931	19.44	13.9		s	521	385	19.40	2.1		c
482	1939	18.90	3.1		c	522	535	18.91	6.0		c
483	1942	19.40	6.1		c	523	638	19.30	6.7	4.2	b
484	1943	19.30	2.6	2.8	b	524	659	19.00	2.5		c
485	1946	19.20	4.7	3.3	b	525	669	19.20	2.2		c
486	1954	19.18	9.5	3.8	b	526	688	19.15	84		s
487	1964	18.80	38		s	527	781	18.70	4.7		c
488	1973	18.57	6.2	2.8	d	528	809	18.90	7.0		s
489	1974	19.24	12.2	3.9	b	529	836	18.60	4.2		c
490	1976	19.24	1.9		c	530	911	19.18	30	5.0	d
491	1979	18.00	9.9	3.9	b	531	920	17.70	6.6	3.8	d
492	1987	19.40	10.0	4.8	b	532	1090	19.40	5.3		s
493	1990	18.74	5.4	3.3	b	533	1127	19.50	21		c
494	1991	18.37	5.1	3.9	b	534	1270	18.20	18.1	4.9	d
495	1992	17.42	4.8		s	535	1273	17.00	2.8	3.7	d
496	2002	19.24	10.8	4.3	b	536	1285	19.18	3.1		c
497	2003	19.47	3.7	2.7	b	537	1294	18.40	16.8	6.4	b
498	2022	16.10	3.5	3.8	d	538	1332	18.40	36	5.6	d
499	2025	19.00	3.0	2.3	b	539	1517	18.80	5.0		s
500	2031	18.95	11.3		s	540	1591	17.89	3.7	3.5	d
501	2043	18.90	23	4.8	b	541	1624	19.00	5.7	4.1	b
502	2059	19.10	3.1	2.5	b	542	1647	18.60	4.0		c
503	2067	18.10	2.6		c	543	1662	18.70	3.8		c
504	2068	19.44	4.4		c	544	1763	18.80	22		s
505	2075	19.00	8.6		c	545	1879	17.76	2.1	3.3	b
506	2077	18.70	32	5.3	b	546	1880	17.20	17.4		s
507	2085	19.30	50		s	547	1908	18.70	6.5		s
508	2086	17.90	5.3	3.6	b	548	2004	19.30	120	7.2	d
509	2087	19.23	29		s	549	2143	18.04	21.3		s
510	2091	18.62	13.6		s						
511	2102	18.10	2.9	4.1	b						
512	2103	17.94	34		s						
513	2107	18.00	6.6	2.8	d						
514	2117	18.40	7.4		c						
515	10	17.85	3.1	3.3	b						
516	60	18.30	140	6.5	d						
517	104	17.20	77		s						
518	266	19.10	2.1	2.9	b						
519	286	17.89	8.1	4.6	b						
520	349	18.83	2.9	3.6	b						

Table 2. The mean parameters and their rms of the emission objects

Type	n	V	$U-B$	$B-V$	$V-\mathrm{H}\alpha$	SB	S	$d\ (''$)	$W'_{\mathrm{H}\alpha}$ (Å)
s	81	18.23	−0.78	0.08	2.26	277	19.7		273
		0.10	0.04	0.03	0.11	9	2.0		38
d	154	18.35	−0.85	0.08	2.52	180	28.0	4.93	558
		0.07	0.03	0.02	0.11	5	2.9	0.14	82
b	180	18.83	−0.68	0.04	1.65	75	6.9	4.08	120
		0.03	0.02	0.02	0.05	2	0.6	0.09	11
c	117	18.85	−0.82	0.05	1.60	625	4.2		101
		0.04	0.03	0.02	0.05	218	0.2		8
zs	17	18.55	−0.98	0.01	3.14		93		824
		0.20	0.07	0.09	0.36		34		342

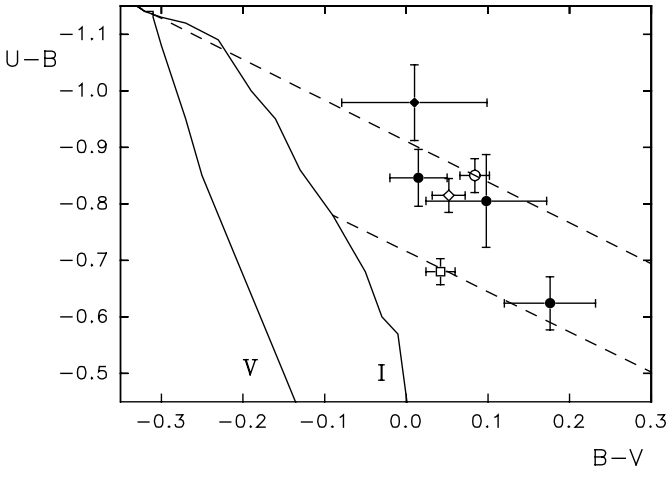

Fig. 4. Two–colour diagram for stars (full circles), from the bottom upwards for bright, mean and weak groups, respectively; diffuse nebulae (circle), bubbles (square), common intermediate objects (rhomb) and zs type objects (filled rhomb). Consequences of I and V luminosity classes and their reddening lines are shown

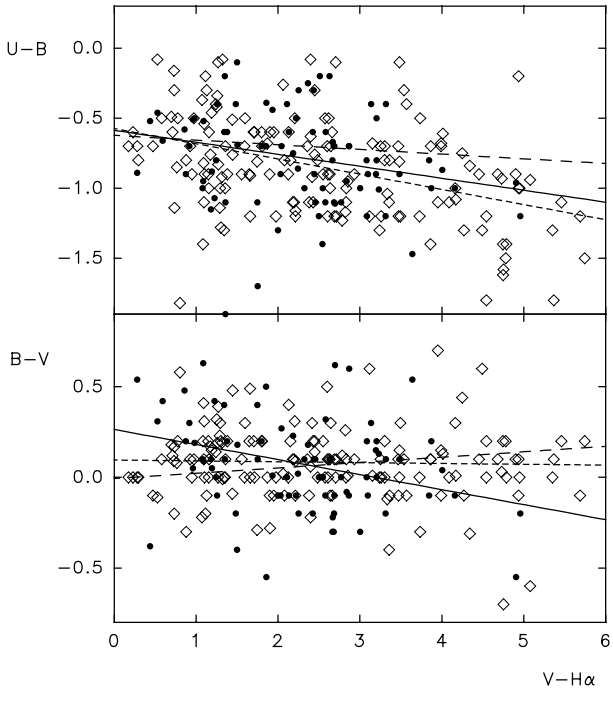

Fig. 5. Standard indices as a function of $V - H\alpha$. Here, as in the following figures, stars are marked with dots and solid lines, diffuse nebulae – rhombs and dotted lines. The b nebulae (long–dashed lines) are not presented

in M 33 should terminate at 10 pc. For instance, in the Galaxy, compact H II regions of smaller size occur fairly often (Wink et al. 1982). Therefore the position of the maximum in our sample is also explained by the selection effect in isolating nebulae. The losses of our nebulae caused by the selection originate at sizes smaller than $3''-4''$.

In Fig. 7b a total distribution of sizes of nebulae from the two lists is shown. It appears quite smooth and continuous. From comparison of Figs. 7a and 7b it can be concluded that in the region of sizes $5''-7''$ many nebulae are missing in our sample; the incompleteness of the list here is $\gtrsim 50\%$. For nebulae with sizes greater than $7''$ (25 pc) the incompleteness of our list sharply increases. This is probably due to the fact that a single early star is incapable of ionizing larger H II regions. Such regions are ionized by groups of stars or OB associations, which were, naturally, disregarded when compiling the catalogue by IFM. As it was shown (Ivanov 1991), the size distribution of OB associations in M 33 fits well the distribution of H II regions from the list of Courtes et al. (1987).

In Fig. 8 the nebulae b and d from Table 1 are shown separately. The distribution peaks correspond to $3''.2$ for bubbles and $3''.7$ for diffuses, their mean sizes (Table 2) are $4''.1$ and $4''.9$ correspondingly. Our nebulae d are, on the average, greater, their distribution is asymmetric. The distribution of bubbles is much more symmetric, their sizes are basically in the range $2''-6''(7-20$ pc) with the mean value 14 pc, the distribution extends to 40 pc. It is noteworthy that the known galactic ring structures around WR and Of stars are about of the same size (Lozinskaya 1992) they are in range $3 \div 30$ pc. The sizes of galactic SN remnants have a somewhat greater dispersion — from 7 to 50 pc.

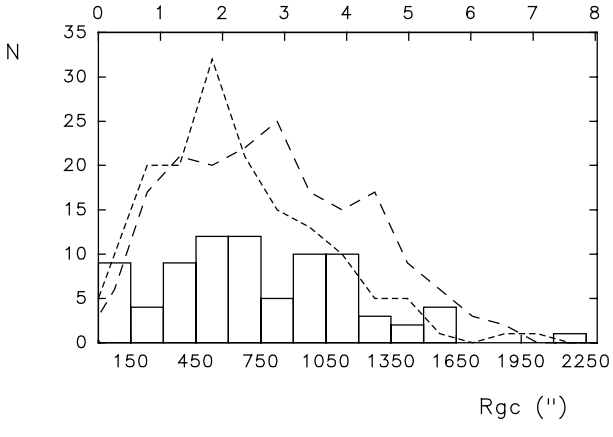

Fig. 6. Distribution of the objects in intervals of galactocentric distance, solid line — stars, dotted line — diffuse nebulae, long–dashed line — b type nebulae. The upper axis is graduated in kpc

In the list of Courtes et al. (1987) 23 bubbles are presented whose sizes range from 70 to 250 pc. Based on the character of distributions of b nebulae from these two samples it was suggested (see for more details Fabrika & Sholukhova 1997), that our bubbles of small sizes and the bubbles of Courtes et al. (1987) are of different physical nature, whereas the bubbles with sizes $> 6''$ may belong to the same population as these of Courtes et al. (1987).

Up to the sizes $\lesssim 30''$, the sample of Courtes et al. (1987) chiefly contains diffuse and compact objects, and

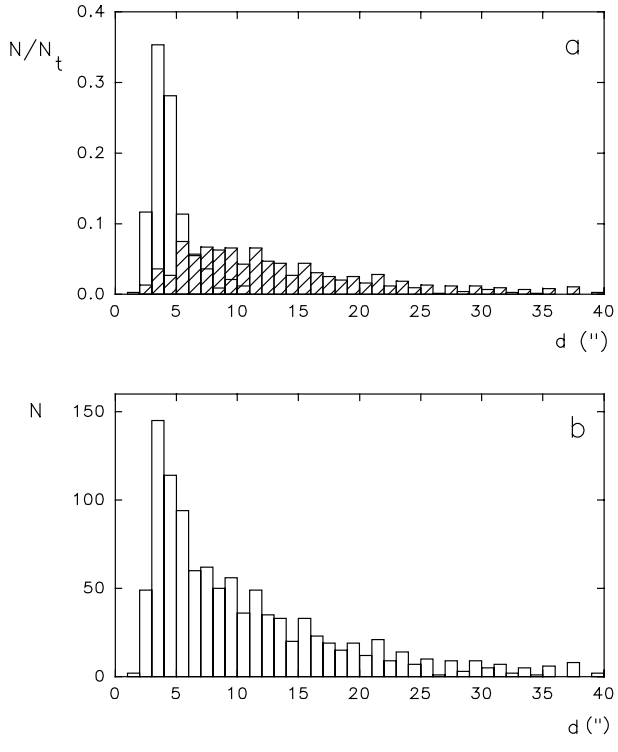

Fig. 7. Size distributions of 748 Hα nebulae from Courtes et al. (1987) (shaded) and our 334 nebulae are shown separately **a)** and as a sum distribution **b)**

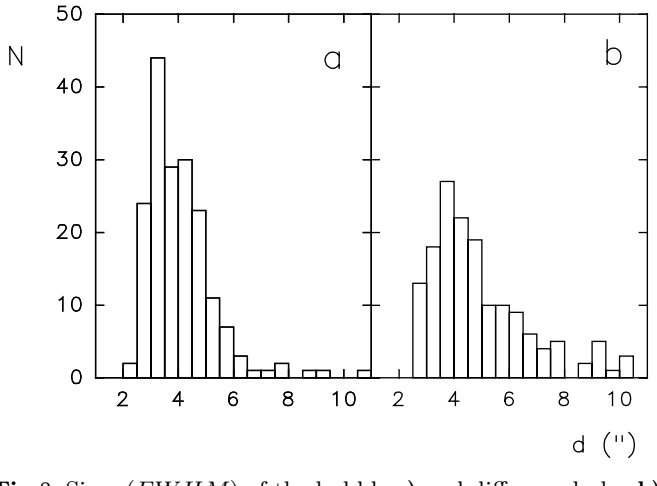

Fig. 8. Sizes ($FWHM$) of the bubble **a)** and diffuse nebulae **b)** from Table 1

the shaded histogram in Fig. 7a actually represents the distribution of objects only of these types. The distribution of objects from both lists looks compatible and supplement each other in Fig. 7. We can suggest that, as different from bubbles, diffuse nebulae of the two lists are likely to belong to the same population.

It can be seen from Fig. 9 that with growing size of the diffuse nebulae their $U-B$ index decreases ($C(U-B,\, d) = -0.097 \pm 0.015$). The figure supports the assumption that size of such a nebula, i.e. H II region, is

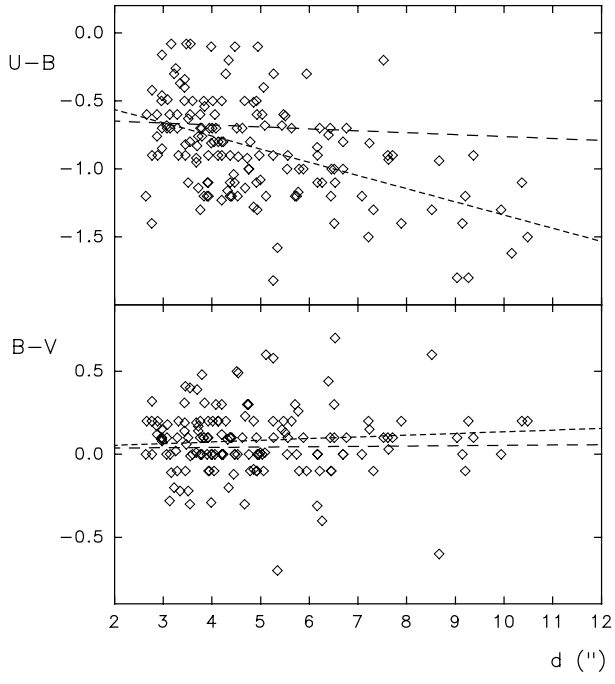

Fig. 9. Colour indices as a function of nebulae sizes. The designations are the same as in Fig. 5

determined by the star temperature. However the mean colours of the diffuses (Table 2) are in agreement with those calculated for an optically thick slab of hydrogen gas with temperature $T \approx 10^4$ K (Kolesov 1996). Comparing the data in Fig. 9 with the calculations one may conclude that with growing size of the diffuse nebulae their gas excitation temperature (or optical thickness) drops. It may also follow from the figure that with the growing size the Balmer line emission becomes brighter (or the contribution of the nebula spectrum to a total flux grows). The relations for bubble nebulae in Fig. 9 are insignificant. It is not improbable, however, that the bubbles get cooler and their gas temperature drops as the size increases (or the $F(\mathrm{H}\alpha)$ flux increases, Fig. 5) since $U-B$ decreases, while $B-V$ grows. The significance of the relationships for the nebulae of type b allows this effect just to be suspected.

We present in Fig. 10 relationships between Hα surface brightness (SB) of b and d nebulae and their galactocentric distance. Besides the apparent separation of the nebulae into two groups in SB (it was discussed above), the brightness of bubbles is clearly seen to decrease with the distance from centre, $\mathrm{C}\,(SB, R_{\mathrm{gc}}) = -0.024 \pm 0.004$. The increasing brightness of the diffuses is also noticeable, but this is not so significant. The nebulae of d type in this figure show a considerable scatter. One can see that the diffuse nebulae whose surface brightness is not high ($SB \lesssim 150$), do not show SB to depend on the distance, while in brighter objects SB is likely to grow with distance. In other words, the bright diffuse objects exhibit the dependence of SB on R_{gc}.

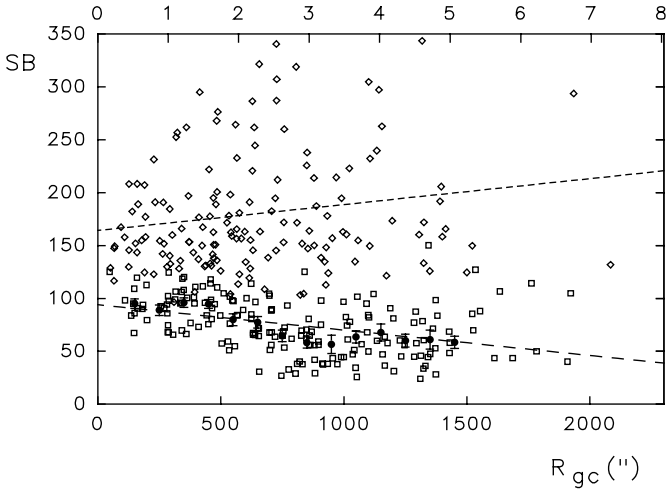

Fig. 10. Hα surface brightness versus galactocentric distance of the nebulae. For bubbles (squares) the average values and their rms deviations in 100″ bins are shown also. The upper axis is graduated in kpc

It is evident from geometrical considerations that with increasing size of diffuse nebula its surface brightness rises, whereas it diminishes (or remains approximately constant) in a case of a bubble. The increase in SB of the bright diffuse nebulae with the galactic distance in Fig. 10 is quite consistent with results of Searle (1971), Smith (1975), Shields & Searle (1978), where the strengthening of ionizing radiation along the radius of M 33 was discussed. This was derived in analysis of line intensity ratios [O III]/Hβ and Hα/[S II] with radius. The relationship for the nebulae of type d in Fig. 10 agrees with the assumption that the average temperature of hot stars grows with distance from the galactic nucleus. These relationships could be also explained by a chemical composition gradient, the more so that such a gradient has been determined in M 33 (Kwitter & Aller 1981).

A value $W'_{\rm H\alpha}$ we obtained above assumes Hα line flux originating in nebula, while the underlying continuum flux is of stellar origin. This value is a direct function of the ratio of the star's luminosity beyond Lyman limit to the luminosity in V band, i.e. the star's temperature. In the diffuse nebulae $< W'_{\rm H\alpha} > = 560 \pm 80$ Å. From calculations of Churchwell & Walmsley (1973) this corresponds to effective spectral class of ionizing stars O 9.5. The nebula size (Stromgren radius) is defined, in turn, by the luminosity and temperature of the star, as well as by a surrounding gas density. Taking the mean electron density $N_{\rm e} = 1\,{\rm cm}^{-3}$ and using data of Prentice & Haar (1969) for B0 stars, find the H II region sizes have to be from a few pc to tens of pc depending on luminosity class of the star. These values agree with typical sizes of the d type nebulae in our list.

The bubbles show inverse relationship between SB and $R_{\rm gc}$. Such behaviour is due to the drop of interstellar gas pressure caused by the decrease of gravitational potential with increasing distance from the centre. The size of a bubble is defined by its internal energy and by the pressure of surrounding gas. In the case of envelopes around WR stars, the total energy of a bubble is the energy of gas ejected during the time of WR stage. Accordingly, in the case of SN remnant this is the kinetic energy of ejecta. With a possible considerable dispersion of those values the decrease in pressure with distance throughout the galaxy accounts for the relationship in Fig. 10. This effect was noticed earlier by Boulestex et al. (1974). They found that sizes of large, 30″– 60″, bubbles grow with radial distance.

One can readily see (Fig. 10) together with the average fall of SB of bubbles with the galactic radius, this relation itself is not monotonic. There are two pronounced peaks near 400″– 600″and 1000″– 1200″. In these distance intervals the bubbles surface brightness rises as if the interstellar medium pressure is maximum there. In order to emphasize this, we present the mean values of SB in 100″ bins denoted by the filled symbols. The deviations from the linear trend are considerable and amount to no less than $3-4\ \sigma$ in separate bins. These features are consistent with those discussed above when analyzing Fig. 6, namely: there are more emission stars and diffuse nebulae in about the same distance regions (spiral arms?), but the number of bubbles is smaller there. It can be seen in Fig. 10 that the latter have an enhanced surface brightness in these particular distances, which may be connected with the increase in interstellar gas pressure. Humphreys & Sandage (1980) isolated up to 10 arms in the M 33 disk. This is quite possible because of non-uniform location of the arms as well as their different curvature that the spiral arms density turns out to be higher in some intervals. On the other hand the existence of ring structures in M 33 may well be assumed. There is a lot of evidence (e.g. Mezger 1970) that such structures do exist in the Galaxy.

We may conclude that the diffuse nebulae are H II regions with an exciting star. These are chiefly situated in the central part of the galaxy, in the regions of enhanced gas density. The sizes of these nebulae in Hα are very sensitive to their central stars temperature. We believe that the brightness and colours of these objects are mainly defined by their stars. On the two–colour diagram (Fig. 4) they follow to the sequence of stars. Hydrogen emission is likely to predominate in their spectra, while nebular lines are weak. The bubbles are probably composed of a high excitation gas, nebula lines must predominate in their spectra. Their central stars contribution to the total flux of these objects may be insignificant. By their properties we identify these objects with envelopes round WR stars and with supernova remnants.

7. The stars

Among emission stars selected there are objects of different brightness $V = 15\overset{\rm m}{.}5 - 19\overset{\rm m}{.}5$. At a distance modulus

Table 3. Parameters of the stars

V	n	$U-B$ rms	$B-V$ rms	$E(U-B)$ $I\,/\,V$	$E(B-V)$ $I\,/\,V$	A_V $I\,/\,V$	$(U-B)_0$ $I\,/\,V$	$(B-V)_0$ $I\,/\,V$	M_V $I\,/\,V$
< 17.5	20	−0.62	0.18	0.20	0.29	0.96	−0.82	−0.11	−8.3
		0.05	0.06	0.33	0.45	1.48	−0.95	−0.27	
17.5−18.5	21	−0.80	0.10	0.22	0.28	0.91	−1.02	−0.18	−7.3
		0.08	0.07	0.30	0.41	1.35	−1.10	−0.31	
18.5−19.5	40	−0.85	0.01	0.15	0.19	0.62	−1.00	−0.18	−5.9
		0.05	0.04	0.24	0.32	1.04	−1.09	−0.30	−6.3

$24\overset{\mathrm{m}}{.}3$ it is obvious that all of them are early massive stars of different luminosity classes. Because of the great dispersion of luminosities, it was a good plan to divide all the stars into three groups: bright ($V < 17\overset{\mathrm{m}}{.}5$), medium ($17\overset{\mathrm{m}}{.}5 < V < 18\overset{\mathrm{m}}{.}5$) and faint ($18\overset{\mathrm{m}}{.}5 < V < 19\overset{\mathrm{m}}{.}5$). In Table 3 we present star numbers in these groups and mean observed colour indices with their deviations. On the two–colour diagram displayed in Fig. 4, filled circles indicate the groups. The error bars are rms of the mean values. Stellar magnitudes presented by IFM have been calibrated by photoelectric standards and have no noticeable systematic errors. The average scatter is equal to $\sigma(U) = 0\overset{\mathrm{m}}{.}22$, $\sigma(B) = 0\overset{\mathrm{m}}{.}29$ and $\sigma(V) = 0\overset{\mathrm{m}}{.}20$. The error being larger for the objects in compact groups, in isolated objects the individual error does not exceed $0\overset{\mathrm{m}}{.}1$ (IFM).

In Fig. 4 two sequences are shown for stars of luminosity classes I and V as well as two reddening lines (dashed) for B0I and OV stars, respectively (Strajzhis 1977). The slopes of the reddening lines differ insignificantly. For each of these three groups and for two luminosity sequences we have found corrected colour indices $(U-B)_0$ and $(B-V)_0$, colour excesses $E(U-B)$ and $E(B-V)$ and light absorption values $A_V = R \cdot E(B-V)$. The values R (Strajzhis 1977) have been used for sequences I and V separately, but they are very close, $R \approx 3.29$. In Table 3 we present the values obtained for both sequences. For each group of stars the top line in the table conforms to the assumption that their luminosity class is I, the bottom one — class V.

The division of stars into three brightness groups is conventional and needed for a safer determination of their mean characteristics. The apparent difference of the groups in colours justifies the division itself. We have assumed that bright and medium stars should be referred to luminosity class I, faint ones to V. In this case we obtain throughout these three groups very close values of interstellar absorption with the mean value $A_V = 0\overset{\mathrm{m}}{.}97$. However we find below that the bright and medium groups should be only used for the absorption to be determined most reliably. We conclude then from two brighter groups of stars, that the mean value of total interstellar absorption among early stars with Hα emission in M 33 is $A_V = 0\overset{\mathrm{m}}{.}93 \pm 0\overset{\mathrm{m}}{.}05$. This estimate is consistent with results of other authors. Humphreys (1980) gives $A_V = 0\overset{\mathrm{m}}{.}8 \pm 0\overset{\mathrm{m}}{.}07$ for blue supergiants in M 33. From CCD photometry of OB stars Wilson (1990) has found the mean value $< E(B-V) >= 0\overset{\mathrm{m}}{.}3$ ($A_V = 0\overset{\mathrm{m}}{.}9 \div 1\overset{\mathrm{m}}{.}0$). The interstellar absorption in the Galaxy in this direction is $0\overset{\mathrm{m}}{.}2 \div 0\overset{\mathrm{m}}{.}3$ (Sharov 1988; van den Bergh 1991).

All the selected stars are star–like sources in Hα. This emission is the most powerful one in H II spectra and it does not contribute to V band. One may suggest that if even H II regions do exist near these stars, it is hardly probable that their emissions contribute essentially to U, B and V bands. Figure 11 presents the colour–luminosity diagram for three groups of stars from Table 3, where filled circles correspond to the idea that the bright and medium stars are supergiants, while faint group is main sequence stars. The open circles indicate the position of the faint stars as supergiants with $A_V = 0\overset{\mathrm{m}}{.}6$ (Table 3). Bars in the figure correspond both to the colour errors (as in Fig. 4) and the intervals in stellar magnitudes. The curves of different luminosity classes are plotted from compilations of Strajzhis (1977, 1982a). The uppermost curve for hypergiant stars is constructed from data of Lang (1992).

The brightest stars do not conform to any of the classical stellar sequences (Strajzhis 1977, 1982b). The close luminosity class is Ia, in colours they fit on the average to B0Ia–B4Ia. However, the first group stars are essentially brighter ($\triangle M_V = 1\overset{\mathrm{m}}{.}1$) than Ia stars. We conclude that they belong to hypergiants or super–supergiants. LBV stars are found among such stars, in their characteristics they fit well this kind of objects (Humphreys & Davidson 1994). It can be seen in Fig. 11 that they fully satisfy this sequence. Their mean luminosity is $M_V = -8\overset{\mathrm{m}}{.}3$. The mass of such stars is over 60 $M_\odot$. The intermediate group stars, both in colours and in luminosities, conform on average very well to B1Ia supergiants (Fig. 11). Their luminosity is $M_V = -7\overset{\mathrm{m}}{.}3$. Masses of such stars are about $40 - 45\ M_\odot$.

We assumed originally from the equality of absorption values for all three groups that luminosity class of the faint group is V. In that case a great luminosity excess, $\triangle M_V = 2\overset{\mathrm{m}}{.}3$, appears as compared to stars of this type.

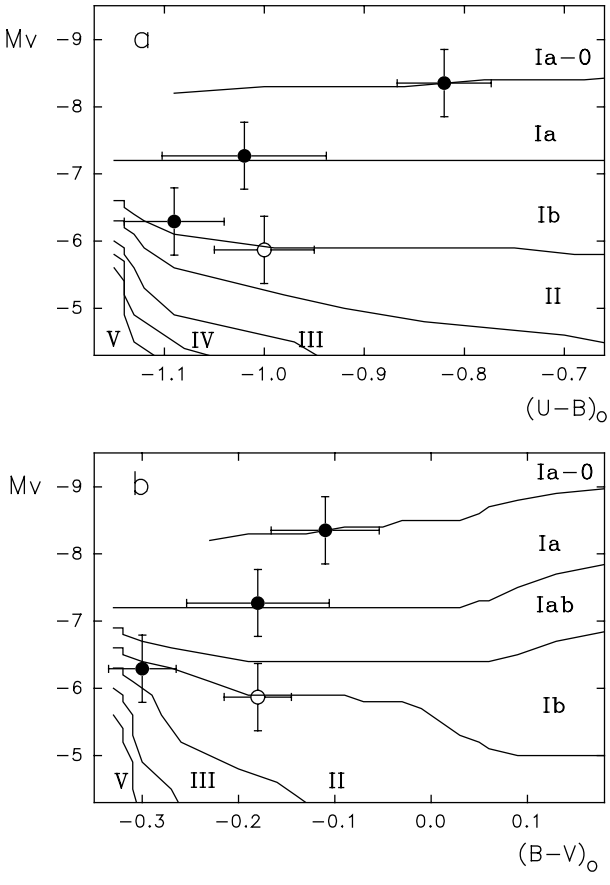

Fig. 11. Colour–luminosity diagram for the bright, mean and weak groups of stars from Table 3. Filled circles show I luminosity class for stars of bright and medium groups, and V class for the faint. Open circle marks position of the faint stars, if their luminosity class is I

If we assume these stars to be of luminosity class III, the excess ($\triangle M_V = 1\overset{\mathrm{m}}{.}4$) remains unexplained all the same. Since a limiting magnitude (IFM) is $V = 19\overset{\mathrm{m}}{.}5$, it is apparent that at $A_V \approx 1\overset{\mathrm{m}}{.}0$ only stars with $M_V \leq -5\overset{\mathrm{m}}{.}8$ will be accessible to us. This practically rules out the appearance of noticeable portion of main sequence stars and giants among the faint group.

It is seen in Fig. 11 that these stars are located on Ib supergiant branch. In this case their absorption is $A_V \approx 0\overset{\mathrm{m}}{.}6$ and the mean luminosity $M_V = -5\overset{\mathrm{m}}{.}9$ (Table 3). They are markedly fainter than Iab supergiants but they fit very well the Ib sequence. From the luminosity and colour indices their average spectral class satisfies completely B1Ib. Masses of such stars are about $20 - 25\ M_\odot$. Obviously, the group of faint stars is not homogeneous, and we discuss their average properties. Both supergiants and the hottest main sequence stars may enter this group.

The mean interstellar absorption of the bright Hα supergiants corresponds to an optical depth of 0.86 (Strajzhis 1977). For the faint group stars this value are 1.5 times as small. This may imply the faint stars are not observable throughout the whole disk of M 33 but only over the near face part of it. Stars of this group are located, on the average, in the near half accross the disk, which takes up 60% of the galaxy disk's cross–section on the line of sight. Hence, the incompleteness of our faint star group (Ib supergiants with Hα emission) is no less than 40%. The incompleteness in general is, naturally, caused by the limiting magnitude $V = 19\overset{\mathrm{m}}{.}5$ in the sample (IFM).

Sholukhova et al. (1997, 1999) carried out a multi-object follow up spectroscopy of a part of object from the list (Table 1). The spectra were obtained in Hα line region. A main goal of the observations was to isolated objects with broad Hα, as a broad emission line suggests that it is formed (completely or partially) in stellar atmosphere. Among 170 objects studied in the follow up spectroscopy, 57 show a broad Hα emission. In this way we may obtain a new list of the most reliable candidates. The authors took spectra of 7 stars (s) from the bright group and found the mean Hα emission width is $FWHM = 310 \pm 40$ km s^{-1}, among 7 stars studied of the medium group $FWHM = 165 \pm 90$ km s^{-1} and 13 stars of the faint group have $FWHM = 115 \pm 50$ km s^{-1}. 32 objects of b type and 39 objects of d type have shown correspondingly 110 ± 30 km s^{-1} and 90 ± 35 km s^{-1}. The high dispersion of the line widths is because the morphological groups are not very homogeneous and both the stellar atmospheres and the H II regions have to contribute to the total Hα emission. In spite of these we see that the objects, separated only from the morphological criteria, clearly differ in Hα line width. The stars have broader Hα, this confirms that their Hα is completely or partially intrinsic. The decrease in the $FWHM$ in the stars as one goes from the bright group to the faint one corroborates the conclusion that the nebulae contribution to the spectrum increases with declining brightness of the star.

Thus, we conclude the blue Hα emission stars in our list are supergiants of luminosity classes Ia–Ib. We also conclude that the group of 20 brightest stars is well consistent with hypergiants or LBV type stars. The mean interstellar absorption estimated from the bright supergiants which are visible across the entire galaxy disk depth is $A_V \approx 0\overset{\mathrm{m}}{.}93$. Light absorption of the faintest stars is $A_V \approx 0\overset{\mathrm{m}}{.}6$.

8. Conclusion

In this paper identification and photometry of blue stellar objects in Hα images of the galaxy M 33 have been performed. Out of 2332 blue stars of the cataloque by IFM we have managed to identify and measure 1619 objects in Hα. On the Hα flux — V magnitude diagrams the stars without noticeable emission form a nonemission sequence above which emission line objects are located. Their Hα emission may be both the intrinsic radiation of the star's

envelope and the radiation of a compact H II region around the star. All in all 549 objects have been isolated by the criteria of the Hα excess. Based on the relationships between a size and Hα line flux, a size and Hα surface brightness, it has been found that 334 or 60% of the candidate stars are extended objects in Hα having the characteristics of diffuse nebulae or bubbles. There have also been isolated 81 stars and 117 compact star–like emission sources.

The objects selected could be considered as candidates for supergiants, hypergiants, WN and SS 433 type stars. All of them are brightest stars in M 33 and they are mainly star–like objects in U, B and V bands (IFM). The isolated Hα morphological groups differ in a wide variety of characteristics: luminosities, colours, fluxes and suzes in Hα, and distribution over M 33. There is evidence that the location and properties of the Hα nebulae depend on the density and pressure of interstellar gas and are related with spiral arms.

The diffuse nebulae are H II regions with an exciting star. Hydrogen emission is likely to be dominant in their spectra and nebula lines are weak, their colours may be defined by the star. The bubbles are probably composed of high excitation gas and nebula lines must predominate in their spectra. The contribution of the central star to the total flux of these objects may be insignificant. By their properties, we identify these objects with envelopes round WR stars or supernova remnants. The group of common objects comprises objects of all types, but, basically, these are stars and compact diffuse nebulae. The diffuse and large bubble–type nebulae in our list are likely to belong to the same assemblies of nebulae listed by Courtes et al. (1987), but they are small–sized, mainly $7 - 20$ pc.

Among the selected emission stars we isolate a group of the 20 brightest stars which, in their average characteristics, conform to the blue hypergiants or LBV type objects. The stars of intermediate luminosity comply with the bright supergiants of average spectral class B1Ia. The interstellar absorption for these two types of stars is $A_V = 0^{\rm m}.93 \pm 0^{\rm m}.05$. The faintest stars have in main to be blue Ib supergiants. The mean absorption of these stars is $A_V = 0^{\rm m}.6$, they are not observable across the whole disk but only in its nearest to the observer part. The number of the latter stars is restricted by the limiting stellar magnitude in the original list.

Acknowledgements. The authors thank V.V. Vlasyuk for providing us with program packages for processing images, G.R. Ivanov for providing the catalogue prior to publication, S.N. Dodonov for Hα photographs made available, to N.A. Tikhonov, A.I. Zakharov and T.B. Georgiev for helpful discussions. This work has been supported by a grant N 3–13 of the Program "Astronomy" RAS, a grant A–02–021 of the ESO C&EE Program and the RFBR grant 97-02-16423.

References

Allen K.U., 1973, Astrophysical quantities. The Athlone Press, University of London
Boulestex J., Courtes G., Laval A., Monnet G., Petit M., 1974, A&A 37, 33
Calzetti D., Kinney A.L., Ford H., Doggett J., Long K.S, 1995, AJ 110, 2739
Churchwell E., Walmsley C.M., 1973, A&A 23, 117
Courtes G., Petit H., Sivan. J.-P., Dodonov S., Petit M., 1987, A&A 174, 28
Fabrika S.N., Sholukhova O.N., 1995, Ap&SS 226, 229
Fabrika S.N., Sholukhova O.N., Zakharova S.A., 1997, Bull. Special Astrophys. Obs. 43, 133
Fabrika S.N., Sholukhova O.N., 1997, Bull. Special Astrophys. Obs. 43, 149
de Vaucoulers G., 1959, AJ 130, 728
Humphreys R.M., Sandage A., 1980, ApJS 44, 319
Humphreys R.M., 1980, AJ 241, 587
Humphreys R.M., Davidson K., 1994, PASP 106, 1025
Ivanov G.R., 1991, MNRAS 251, 281
Ivanov G.R., Freedman W.L., Madore B.F., 1993, ApJS 89, 85 (IFM)
Kolesov A.K., 1996, Afz 39, 247
Kwitter K.B., Aller L.H., 1981, MNRAS 195, 939
Lang K.R., 1992, Astrophysical Data: Planets and Stars: New York
Lozinskaya T.A., 1992, Supernovae and Stellar Wind in the Interstellar Medium, New York: American Institute of Physics
Mezger P.G., 1970, in: Becker W., Contopoulos G. (eds.), The Spiral Structure of our Galaxy. IAU Symp., No. 38. Dordrecht: D. Reidel Publ. Comp.
Prentice A.J.R., ter Haar D., 1969, MNRAS 146, 423
Sabbadin F., Rafanelli P., Bianchini A., 1980, ApJS 39, 97
Searle L., 1971, AJ 168, 327
Smith H.E., 1975, AJ 199, 591
Strajzhis B., 1977, Mnogotsvetnaya fotometriya zvezd, Vil'nyus: Mokslas
Strajzhis B., 1982a, Bull. Vil'nyus Obs. 78, 43
Strajzhis B., 1982b, Zvezdy s defitsitom metallov, Vil'nyus: Mokslas
Sharov A.S., 1988, Spiral'naya galaktika Mes'e 33, M.: Nauka
Sholukhova O.N., Fabrika S., Vlasyuk V.V., Burenkov A.N., 1997, Astron. Lett. 23, 458
Sholukhova O.N., Fabrika S., Vlasyuk V.V., Dodonov S.N., 1999, Astron. Lett. 25, 14
Shields G.A., Searle L., 1978, ApJ 222, 821
van den Bergh S., 1991, PASP 103, 609
Wilson D.C., 1990, Ph.D. Dissertation, California Institute of Technology
Wink J.E., Altenhoff W.J., Mezger P.G., 1982, A&A 108, 227
Zickgraf F.-J., Humphreys R.M., 1991, AJ 102, 113